

# Phosphate Doping into Monoclinic BiVO<sub>4</sub> for Enhanced Photoelectrochemical Water Oxidation Activity\*\*

Won Jun Jo, Ji-Wook Jang, Ki-jeong Kong, Hyun Joon Kang, Jae Young Kim, Hwichan Jun, K. P. S. Parmar, and Jae Sung Lee\*

Hydrogen has been touted as an energy carrier of the future because it combines with oxygen to produce only water with no greenhouse gases or other pollutants. For hydrogen to play the role, it must be produced in a sustainable manner from a renewable energy source, such as solar energy.<sup>[1]</sup> Unlike the electricity produced from the most common photovoltaic cells, hydrogen could store the solar energy in the form of chemical energy. One of the most attractive solar energy conversion reactions is the photoelectrochemical (PEC) or photocatalytic water splitting directly to H<sub>2</sub> and O<sub>2</sub>. Since its initial demonstration by Fujishima and Honda with a TiO<sub>2</sub> electrode under ultraviolet light,<sup>[2]</sup> there has been steady progress in this field in search of semiconductor photocatalytic electrode materials that work under visible light irradiation for ample solar light absorption. However, the photocatalysts with high efficiency, durability, and economic feasibility are still elusive.<sup>[3,4]</sup>

Scheelite-monoclinic BiVO<sub>4</sub> (*m*BiVO<sub>4</sub>) is a well-known photocatalyst, which absorbs visible light owing to a suitable band-gap energy ( $E_g \approx 2.4$  eV).<sup>[5,6]</sup> It is also nontoxic and chemically stable in aqueous solution under irradiation. However, pristine *m*BiVO<sub>4</sub> usually shows a low photocatalytic activity owing to poor charge-transport characteristics<sup>[7]</sup> and the weak surface adsorption properties.<sup>[8]</sup> Numerous attempts have been made to improve the photocatalytic activity of BiVO<sub>4</sub>, including heterojunction structure formation,<sup>[7,9,10]</sup> loading co-catalysts,<sup>[11–13]</sup> and impurity doping.<sup>[8,14,15]</sup>

Impurity doping, that is, the addition of a small percentage of foreign atoms in the regular crystal lattice of semiconductors, produces dramatic changes in their electrical properties by increasing their electron or hole densities. In photocatalysis by BiVO<sub>4</sub>, for example, doping with molybdenum to

replace a small fraction of vanadium was found to improve the photocatalytic activity for water oxidation.<sup>[8,14,15]</sup> Phosphorus is a typical dopant for silicon or germanium to make it an n-type semiconductor. However, it has been rarely used as dopant for semiconductor photocatalysts. This is rather surprising because other non-metallic elements, such as N, C, and S, have been widely used as anionic dopants for photocatalysts to reduce their band-gap energies.<sup>[16]</sup>

In the present work, for the first time we doped phosphorous into the vanadium sites in the host lattice of BiVO<sub>4</sub>, replacing some of the VO<sub>4</sub> oxoanions in BiVO<sub>4</sub> with PO<sub>4</sub> oxoanions. Oxoanion doping into the photocatalyst is to the best of our knowledge also a new concept. Herein we report effects of PO<sub>4</sub> oxoanion doping on the photoelectrochemical or photocatalytic behavior of *m*BiVO<sub>4</sub> under visible-light illumination. The PO<sub>4</sub> oxoanion doping did not bring about significant changes in the optical absorption behavior and crystal structure of *m*BiVO<sub>4</sub>. When an appropriate amount PO<sub>4</sub> oxoanion was doped, however, the activity of photoelectrochemical water oxidation increased very significantly by a factor of about 30. The origin of the enhanced photoelectrochemical properties of PO<sub>4</sub> oxoanion-doped BiVO<sub>4</sub> was elucidated by using electrochemical impedance spectroscopy (EIS) and density functional theory (DFT) calculations.

The XRD patterns of pristine BiVO<sub>4</sub> and three PO<sub>4</sub>-doped BiVO<sub>4</sub> samples with different target atom ratios (0.5 %, 1 %, and 5 %) are shown in Figure 1a. These four patterns are identical to that of pure monoclinic BiVO<sub>4</sub> (clinobisvanite; space group: *I*2/a, JCPDS card No. 014-0688) without any impurity phase, such as BiPO<sub>4</sub> and oxides of bismuth or vanadium. Figure 1b exhibits the magnified view of (121) and (040) peaks, which show gradual shifts of peaks toward lower angles with increasing PO<sub>4</sub> oxoanion doping level. The 5 % PO<sub>4</sub>-doped sample shows the largest peak shift by 0.10°. The full-width at half-maximum (FWHM) also gradually increases by 11 % compared with pristine BiVO<sub>4</sub>, reflecting the increased strain or reduced grain size of the doped photocatalyst. These XRD results indicate that P<sup>5+</sup> has been well inserted into V<sup>5+</sup> sites of the host BiVO<sub>4</sub> lattice without forming any segregated impurity phase.<sup>[17]</sup>

The UV/Vis absorption spectra of the pristine and three doped BiVO<sub>4</sub> samples are illustrated in Figure 1c. The shape of the UV/Vis absorption spectra of the four samples are almost the same despite PO<sub>4</sub> doping. The optical band-gap energies of the four samples were estimated from the absorption spectra by using the following relationship:  $\alpha h\nu = A(h\nu - E_g)^{n/2}$  where  $\alpha$ ,  $h\nu$ ,  $A$ , and  $E_g$  are the absorption coefficient, the photon energy, constant, and the optical band-

[\*] W. J. Jo,<sup>[†]</sup> Dr. J.-W. Jang,<sup>[†]</sup> H. J. Kang, J. Y. Kim, Dr. H. Jun, Dr. K. P. S. Parmar, Prof. J. S. Lee  
Department of Chemical Engineering and Division of Advanced Nuclear Engineering, Pohang University of Science and Technology (POSTECH)  
San 31, Hyoja-dong, Pohang 790-784 (Korea)  
E-mail: jlee@postech.ac.kr

Dr. K.-j. Kong  
Korea Institute of Chemical Technology  
100 Jang-dong, Yuseong-gu, Daejeon, 305-343 (Korea)

[†] These authors contributed equally to this work.

[\*\*] This research was supported by the Hydrogen Energy Centre (a Frontier Research Program of NRF, Korea), the Korean Centre for Artificial Photosynthesis (NRF-2011-C1AAA001-2011-0030278), WCU, Brain Korea 21, and A3 foresight programs (NRF, Korea).

Supporting information for this article is available on the WWW under <http://dx.doi.org/10.1002/ange.201108276>.

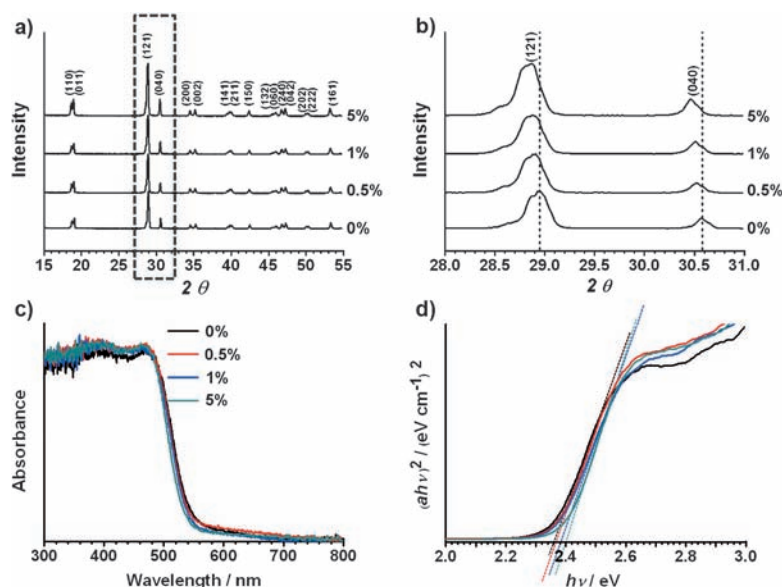


**Figure 1.** a) X-ray diffraction of pristine BiVO<sub>4</sub>, and 0.5%, 1%, and 5% PO<sub>4</sub>-doped BiVO<sub>4</sub>; b) magnified peaks of (120) and (040) planes. c) UV/Vis absorption spectra and d) Tauc plot of bare BiVO<sub>4</sub>, and 0.5, 1, and 5% PO<sub>4</sub>-doped BiVO<sub>4</sub>.

gap energy, respectively. The value of  $n$  depends on whether the transition is direct ( $n=1$ ) or indirect ( $n=4$ ), and it was determined to be unity from the absorption spectra. The band-gap energy was determined by extrapolating the linear part of  $(\alpha h\nu)^2$  vs.  $h\nu$  plot to the energy axis at  $a=0$  as shown in the Figure 1d. According to the Tauc plot, the optical band-gap energies of the four samples are not much different, yet they showed systematic increase with P doping level, that is, pristine BiVO<sub>4</sub> (ca. 2.36 eV), 0.5% P (ca. 2.37 eV), 1% P (ca. 2.38 eV), and 5% P (ca. 2.40 eV). The small difference in band gap will be discussed based on the results of DFT calculations.

The morphology and microstructure of the pristine and PO<sub>4</sub>-doped samples observed by FESEM are exhibited in Figure S1 of Supporting Information. The close inspection of the images reveals that the particle shape of the four samples is an irregular polyhedron and the morphology and size distribution of 0.5, 1% PO<sub>4</sub>-doped BiVO<sub>4</sub> were similar to those of pristine BiVO<sub>4</sub>. However, for 5% PO<sub>4</sub>-doped BiVO<sub>4</sub>, average size of BiVO<sub>4</sub> particles was much smaller than that of pristine BiVO<sub>4</sub> (Supporting Information, Figure S1d inset). When a large amount of PO<sub>4</sub> is doped into the lattice of BiVO<sub>4</sub>, it seems to interfere with the crystallization of BiVO<sub>4</sub>, making average size of BiVO<sub>4</sub> smaller. This is also consistent with the increased FWHM of (121) and (040) peaks for the heavily doped sample.

The real atomic ratios of vanadium to phosphorus of the three PO<sub>4</sub>-doped BiVO<sub>4</sub> samples were determined by the ICP analysis. Table S1 of Supporting Information indicates that the actual concentrations of vanadium of the three samples are less than those introduced initially during the synthesis. It appears that the PO<sub>4</sub> oxoanion not doped into the BiVO<sub>4</sub> lattice has been dissolved in water and removed during the purification step.

It is possible that the PO<sub>4</sub> anion is present as BiPO<sub>4</sub> forming a heterojunction with BiVO<sub>4</sub> instead of doping into the BiVO<sub>4</sub> lattice. To check the existence of BiPO<sub>4</sub>, we performed SEM-EDS point analysis several times, especially on the small particles scattered over the surface of a large BiVO<sub>4</sub> particle (Supporting Information, Figure S1). The concentration of phosphorus in 0.5% and 1% PO<sub>4</sub>-doped BiVO<sub>4</sub> was below the detection limit of SEM-EDS, yet phosphorous contents in 5% PO<sub>4</sub>-doped BiVO<sub>4</sub> (3.5%) was comparable with the actual doping amount (Supporting Information, Figure S2). This indicates that many small particles on the surface of a large BiVO<sub>4</sub> particle are not BiPO<sub>4</sub> but PO<sub>4</sub>-doped BiVO<sub>4</sub>.

To further investigate the state of the PO<sub>4</sub> doping, HR-TEM EDS elemental mapping was carried out. Figure 2a shows a high-angle annular dark-field (HAADF) image of a 0.5% PO<sub>4</sub>-doped BiVO<sub>4</sub> particle. The EDS elemental maps in Figure 2b–e demonstrate that Bi, V, P, and O are distributed homogeneously within the 0.5% PO<sub>4</sub>-doped BiVO<sub>4</sub> particle. The homogeneous distribution of the four elements were also confirmed in 1% and 5% PO<sub>4</sub>-doped samples (Supporting Information, Figure S3, S4). These results show that the PO<sub>4</sub> oxoanion has been doped into the BiVO<sub>4</sub> lattice well without producing any segregated-phase-like vanadate, bismuth oxides, or BiPO<sub>4</sub>. Figure 2f shows a lattice spacing of 0.312 nm corresponding to the interplanar spacing of (130) plane of monoclinic BiVO<sub>4</sub>.

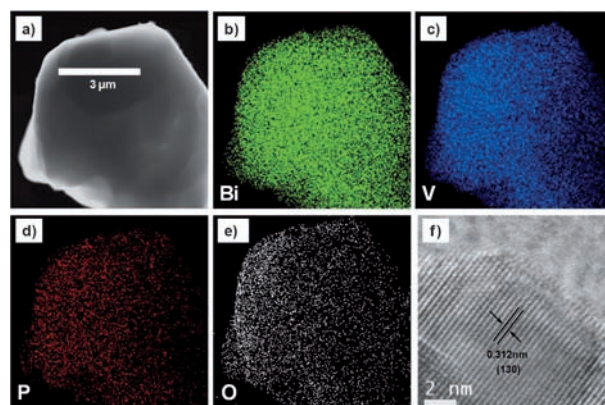


**Figure 2.** a) High-angle annular dark-field (HAADF) image of a 0.5% PO<sub>4</sub>-doped BiVO<sub>4</sub> particle. b)–e) Elemental mapping of b) Bi, c) V, d) P, and e) O. f) HR-TEM image of the doped particle showing the interplanar spacing of (130) plane of monoclinic BiVO<sub>4</sub> (0.312 nm).

Photocurrent density accompanying water oxidation was measured to elucidate the effect of PO<sub>4</sub> doping into the mBiVO<sub>4</sub> lattice under visible light ( $\lambda \geq 420$  nm). All the samples were synthesized in a powder form by urea-precipitation method and they were loaded onto the fluorine-doped tin oxide (FTO) glass by using electrophoretic deposition (EPD) technique. Figure 3a illustrates how photocurrent

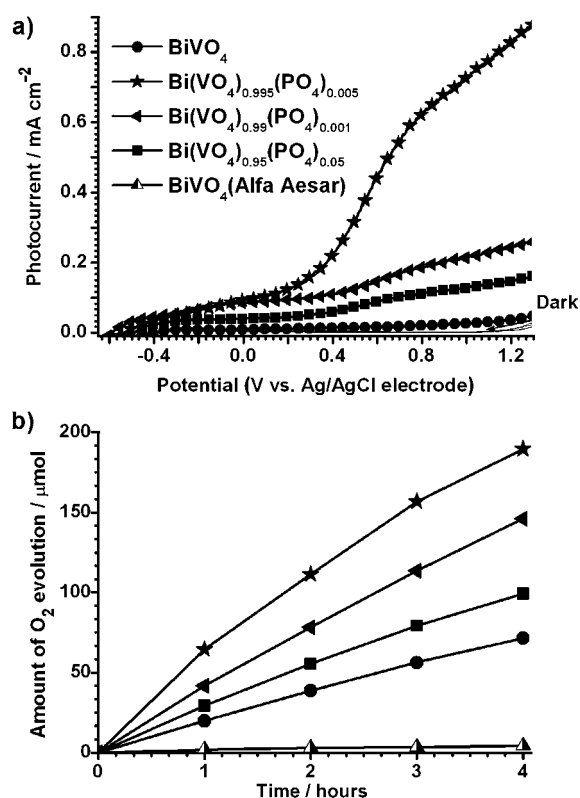


**Figure 3.** a) Photocurrent–potential curves of pristine BiVO<sub>4</sub>, and 0.5, 1, and 5% PO<sub>4</sub>-doped BiVO<sub>4</sub>. The back side of photo-anodes was illuminated with a xenon arc lamp (300 W) fitted with a UV cut-off filter ( $\lambda \geq 420$  nm). b) Photocatalytic water oxidation with bare and PO<sub>4</sub>-doped BiVO<sub>4</sub> under the visible-light ( $\lambda > 420$  nm) irradiation. The photocatalyst powders (0.1 g) were dispersed in aqueous AgNO<sub>3</sub> solution as an electron scavenger.

density of the four photoanodes varies under dark and visible light illumination as applied anodic potential increases from  $-0.6$  V to  $+1.2$  V (vs. Ag/AgCl). Visible light irradiation on photoanodes drives PEC water oxidation reactions to generate photoelectrons, which are collected by the FTO substrate to produce currents:  $2\text{H}_2\text{O}(\text{l}) + h\nu \rightarrow \text{O}_2(\text{g}) + 4\text{H}^+ + 4\text{e}^-$ .

As Figure 3a shows, the photocurrent increased dramatically by PO<sub>4</sub> oxoanion doping. In the best case, the photocurrent ( $0.548 \text{ mA cm}^{-2}$  at  $0.7$  V) produced by 0.5% PO<sub>4</sub>-doped BiVO<sub>4</sub> is about 30 times higher than the photocurrent ( $0.019 \text{ mA cm}^{-2}$  at  $0.7$  V) produced by pristine BiVO<sub>4</sub>. The potential ( $0.7$  V) adopted for comparison corresponds to  $1.23$  V vs. RHE at pH 6.6, which is the theoretical potential necessary for water oxidation:  $E_{\text{RHE}} = E_{\text{Ag/AgCl}} + 0.059 \text{ pH} + E^\circ_{\text{Ag/AgCl}}$  ( $E^\circ_{\text{Ag/AgCl}} = 0.209$  V at  $25^\circ\text{C}$ ). The 1% and 5% PO<sub>4</sub>-doped BiVO<sub>4</sub> anodes also showed much enhanced photocurrents relative to the pristine BiVO<sub>4</sub> electrode, but they were much less than that for 0.5% PO<sub>4</sub>-doped BiVO<sub>4</sub>.

The photocatalytic water oxidation activity of pristine and PO<sub>4</sub>-doped BiVO<sub>4</sub> photocatalysts were also measured for powder samples in 100 mL of aqueous AgNO<sub>3</sub> solution under visible light irradiation ( $\lambda > 420$  nm). Here, Ag<sup>+</sup> ions from AgNO<sub>3</sub> played the role of an electron scavenger:  $2\text{H}_2\text{O}(\text{l}) +$

$h\nu + 4\text{Ag}^+ \rightarrow \text{O}_2(\text{g}) + 4\text{H}^+ + 4\text{Ag}$ . In line with the trend of photocurrent generation shown in Figure 3a, Figure 3b shows that the largest amount of O<sub>2</sub> is evolved by 0.5% PO<sub>4</sub>-doped BiVO<sub>4</sub>, which is more than triple the amount of O<sub>2</sub> evolved by bare BiVO<sub>4</sub>. The order of activity was also the same: pristine BiVO<sub>4</sub> < 5% PO<sub>4</sub>-doped < 1% PO<sub>4</sub>-doped < 0.5% PO<sub>4</sub>-doped BiVO<sub>4</sub>. It should also be noted that the photocatalytic activities of the four BiVO<sub>4</sub> samples prepared by the urea-precipitation method are much higher than the commercial BiVO<sub>4</sub> (Alfa Aesar, 99.9%).

To study the origin of the enhanced PEC and photocatalytic activity, electrochemical behavior of PO<sub>4</sub>-doped BiVO<sub>4</sub> was investigated by the electrochemical impedance spectroscopy (EIS).<sup>[18]</sup> The EIS measurements were carried out at the same condition where semiconductor generated photocurrents ( $0.7$  V vs. Ag/AgCl, visible light) to relate the impedance response directly to the physical processes responsible for the photocurrent generation.<sup>[19]</sup> The results of EIS are presented in Figure 4 in the form of Nyquist plots. Here,

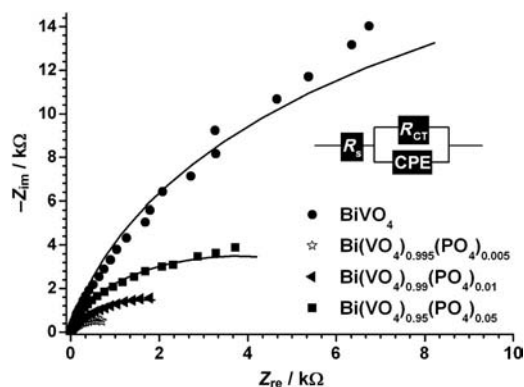


**Figure 4.** Electrochemical impedance spectroscopy measured at  $0.7$  V (vs. Ag/AgCl) in  $0.5 \text{ M Na}_2\text{SO}_4$  solution. The inset shows an equivalent circuit for the photoanodes (see text for details).

the x axis represents the real part of measured impedance and the y axis represents the negative number of the imaginary part of measured impedance. The small dots in the plot represent the experimental data and the solid lines represent the result of fitting these experimental data to the equivalent circuit model. The solid line was fitted by ZSimpWin software using the proposed equivalent circuit model. The Nyquist plot can be interpreted in terms of the equivalent circuit as displayed in the inset. Here, the EIS data were measured using a three-electrode cell system, thus the arc in Nyquist plot represents the charge transfer kinetics on the working electrode. We selected the Randles-Ershler model,<sup>[20]</sup> in which  $R_s$  is the solution resistance, CPE is the capacitance phase element for the semiconductor||electrolyte interface, and  $R_{\text{ct}}$  is the charge transfer resistance across the interface. The smaller value of  $R_{\text{ct}}$  and the larger value of a CPE represent improved charge transport characteristics making favorable environment for charge separation in PEC reactions. An RC circuit represents an interface within the cell. Thus, the arcs in the Nyquist plot are related to charge transfer at the semiconductor||electrolyte interface.



The fitted values of  $R_{ct}$  were 36946, 1206, 3685, and 7651  $\Omega$  for pristine  $\text{BiVO}_4$ , 0.5%, 1%, and 5%  $\text{PO}_4$ -doped  $\text{BiVO}_4$  electrodes, respectively. The fitted value of  $R_{ct}$  for 0.5%  $\text{PO}_4$ -doped  $\text{BiVO}_4$  is about 30 times smaller than that of pristine  $\text{BiVO}_4$ , which show a perfect correlation with the activity trends of both PEC photocurrent generation and photocatalytic  $\text{O}_2$  generation. Thus, the improved charge transfer characteristic of  $\text{PO}_4$ -doped  $\text{BiVO}_4$  is the most important factor responsible for their enhanced photocatalytic performance. The efficient charge transfer at the semiconductor||electrolyte interface suppresses the charge recombination and enhance the efficiency of PEC water oxidation.<sup>[7,21]</sup> When the  $\text{PO}_4$  doping level increased to 1% or 5%, charge transfer resistance increased compared with 0.5%-doped  $\text{BiVO}_4$ . The excessive amount of  $\text{PO}_4$  oxoanion doping seems to form defect sites in the monoclinic  $\text{BiVO}_4$  lattice, which act as electron-hole recombination sites.

By unprecedented  $\text{PO}_4$  oxoanion doping of  $m\text{BiVO}_4$ , we observed a dramatic enhancement of photoelectrochemical water oxidation activity by a factor of about 30. According to the EIS study, this is correlated well with the greatly improved charge transfer characteristics at the semiconductor||electrolyte interface. To elucidate the pronounced doping effect, we performed density functional theory (DFT) calculations of electronic structures.

Clinobisvanite  $\text{BiVO}_4$  has a monoclinic structure (point group:  $C_{2h}$ , space group:  $C2/c$ ) and contains four bismuth or vanadium atoms and sixteen oxygen atoms in the unit cell. Its basic structural unit is constructed by  $\text{VO}_4$  tetrahedron and  $\text{BiO}_8$  dodecahedron, in which bismuth and vanadium atoms are arranged alternately to form a continuous zigzag line on the (221) plane. To obtain self-consistent results, we optimized lattice constants and atomic coordinates, which were obtained by minimizing the total energy, internal stress, and atomic forces. This was done by performing an iterative process in which the cell parameters and coordinates of the atoms are adjusted so that the total energy of the structure is minimized. The relaxation run was considered converged when the force on the atom was less than  $0.01 \text{ eV \AA}^{-1}$ . By doing so, we could obtain stable structures for all of the models. By optimizing the pure clinobisvanite  $\text{BiVO}_4$  structure, we obtained the lattice parameters as follows:  $a = 7.304$ ,  $b = 11.744$ ,  $c = 5.165 \text{ \AA}$ ,  $\beta = 135.003^\circ$ . These parameters were in good agreement with experimental values:<sup>[22]</sup>  $a = 7.258$ ,  $b = 11.706$ ,  $c = 5.084 \text{ \AA}$ ,  $\beta = 134.073^\circ$ . Because doping occurs within bulk  $\text{BiVO}_4$ , our  $\text{PO}_4$  doping model uses the same lattice constants with pristine  $\text{BiVO}_4$ . To avoid the self-interactions of impurity, we adopted the supercell method with sufficient length on all directions. Our  $\text{PO}_4$  doping model consists of two unit cells stacked both along the  $a$  and  $c$  axes in which one of sixteen vanadium atoms is substituted by a phosphorus atom (6.25% of  $\text{PO}_4$  doped), which is comparable to those used in the experiments.

Figure 5a shows the projected density of states (pDOS) of pristine  $\text{BiVO}_4$  and P-doped  $\text{BiVO}_4$ . The calculated band gap of pure  $\text{BiVO}_4$  is about 1.94 eV, which is smaller than the experimental value of 2.36 eV owing to the well-known limitation of DFT, that is, the underestimation of band gap. Upon  $\text{PO}_4$  doping, the band gap becomes slightly larger

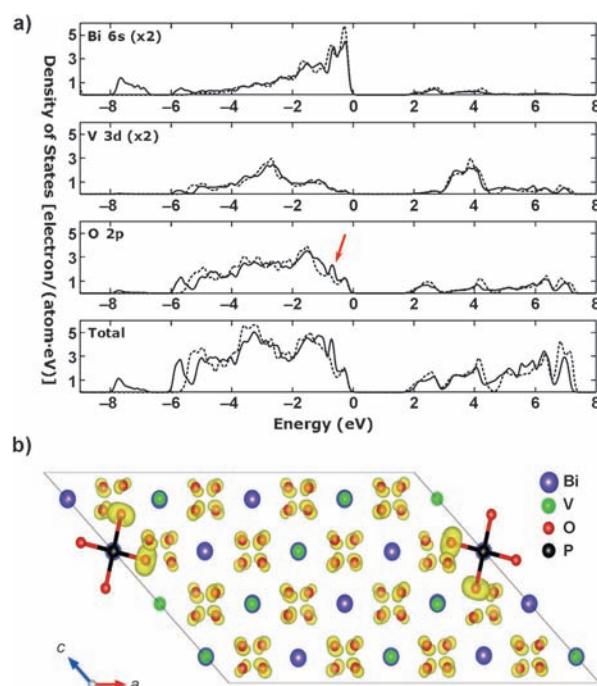


**Figure 5.** a) Total and local partial density of states of monoclinic clinobisvanite  $\text{BiVO}_4$  (.....) and P-doped  $\text{BiVO}_4$  (—). The main effect of P-doping occurs as an additional O2p peak at  $-0.7 \text{ eV}$  (marked by an arrow). The DOS is decomposed into the main electron states of each component. Note the slight increase of band gap upon P substitution. b) Calculated isosurface ( $0.04 \text{ e \AA}^{-1}$ ) of integrated charge density in the range from  $-0.7 \text{ eV}$  to  $E_f$  for P-doped  $\text{BiVO}_4$ . Note the enhancement of  $p_\pi$  states of O bonded with the P atom. Only P–O bonds are shown for clarity.

(1.95 eV for 6.25% doping and 2.00 eV for 25%). This result corresponds well with a slight band-gap change obtained by the Tauc plots. This is also one of the important pieces of evidence that the  $\text{PO}_4$  oxoanion is well-doped.

As is well-known for metal oxides, the top of valence band (VB) is composed of O2p states and conduction band (CB) bottom comes from V3d states. Upon  $\text{PO}_4$  substitution, the DOS of the VB top increases; the ratio of integrated DOS in the energy windows of  $-0.7 \text{ eV}$  from the VB top to total electrons is 4.0% and 5.9% for pristine and  $\text{PO}_4$ -doped  $\text{BiVO}_4$ , respectively. The larger DOS in the VB around the Fermi energy  $E_f$  implies an increase of charge carriers, resulting in lower  $R_{CT}$ . This will lead to higher PEC activity.

The Bader charge analysis<sup>[23]</sup> shown in Figure 5b suggests that the substituted phosphorus atom has a much smaller charge (1.357 electrons) than the vanadium atoms (3.102 electrons). The depleted electrons from the phosphorus atom accumulate around neighboring oxygen atoms, enhancing the non-bonding O2p $_\pi$  states. The calculated Bader charges of oxygen atoms in the  $\text{PO}_4$  tetrahedron slightly fluctuate in the range from 7.406 to 7.453 electrons. The oxygen atoms have charges of 6.966 electrons in the pristine  $\text{BiVO}_4$ . The length of the P–O bond is 1.563  $\text{\AA}$ , which is slightly smaller than the V–O bond (1.737  $\text{\AA}$ ). Owing to the lattice strain imposed by the different V–O and P–O bond lengths and the charge redistribution around the dopant, there exists an internal

electric field. This effect is very advantageous for the separation of electron-hole pairs, which can improve the photocatalytic property.

To summarize, we have investigated PO<sub>4</sub> oxoanion doping into mBiVO<sub>4</sub> for the first time. The 0.5 % PO<sub>4</sub>-doped BiVO<sub>4</sub> showed the best photocurrent density, which is about 30 times higher than that of pristine BiVO<sub>4</sub>. The same trend was observed for photocatalytic O<sub>2</sub> evolution rates. EIS measurements revealed that PO<sub>4</sub> oxoanion doping lowered the charge transfer resistance of mBiVO<sub>4</sub> remarkably. Finally, DFT calculations showed increased charge carriers in PO<sub>4</sub>-doped mBiVO<sub>4</sub>. Both results indicate that the origin of the enhanced photoelectrochemical and photocatalytic properties of PO<sub>4</sub> oxoanion-doped mBiVO<sub>4</sub> greatly improves the charge-transfer characteristics of mBiVO<sub>4</sub>.

Received: November 24, 2011

Published online: February 17, 2012

**Keywords:** bismuth · doping · phosphates · photolysis · vanadates

- [1] M. Grätzel, *Inorg. Chem.* **2005**, *44*, 6841–6851.
- [2] A. Fujishima, K. Honda, *Nature* **1972**, *238*, 37–38.
- [3] K. Maeda, K. Domen, *J. Phys. Chem. C* **2007**, *111*, 7851–7861.
- [4] D. Yamasita, T. Takata, M. Hara, J. N. Kondo, K. Domen, *Solid State Ionics* **2004**, *172*, 591–595.
- [5] A. Kudo, K. Omori, H. Kato, *J. Am. Chem. Soc.* **1999**, *121*, 11459–11467.
- [6] S. Tokunaga, H. Kato, A. Kudo, *Chem. Mater.* **2001**, *13*, 4624–4628.
- [7] S. J. Hong, S. Lee, J. S. Jang, J. S. Lee, *Energy Environ. Sci.* **2011**, *4*, 1781–1787.
- [8] W. Yao, H. Iwai, J. Ye, *Dalton Trans.* **2008**, 1426–1430.
- [9] M. Long, W. Cai, H. Kisch, *J. Phys. Chem. C* **2008**, *112*, 548–554.
- [10] H. Q. Jiang, H. Endo, H. Natori, M. Nagai, K. Kobayashi, *Mater. Res. Bull.* **2009**, *44*, 700–706.
- [11] H. Xu, H. Li, C. Wu, J. Chu, Y. Yan, H. Shu, Z. Gu, *J. Hazard. Mater.* **2008**, *153*, 877–884.
- [12] S. Kohtani, M. Tomohiro, K. Tokumura, R. Nakagaki, *Appl. Catal. B* **2005**, *58*, 265–272.
- [13] S. Kohtani, J. Hiro, N. Yamamoto, A. Kudo, K. Tokumura, R. Nakagaki, *Catal. Commun.* **2005**, *6*, 185–189.
- [14] W. Yao, J. Ye, *J. Phys. Chem. B* **2006**, *110*, 11188–11195.
- [15] W. Luo, Z. Yang, Z. Li, J. Zhang, J. Liu, Z. Zhao, Z. Wang, S. Yan, T. Yu, Z. Zou, *Energy Environ. Sci.* **2011**, *4*, 4046–4051.
- [16] R. Asahi, T. Morikawa, T. Ohwaki, K. Aoki, Y. Taga, *Science* **2001**, *293*, 269–271.
- [17] A. Zhang, J. Zhang, *J. Hazard. Mater.* **2010**, *173*, 265–272.
- [18] S. Banerjee, S. K. Mohapatra, P. P. Das, M. Misra, *Chem. Mater.* **2008**, *20*, 6784–6791.
- [19] E. A. Ponomarev, L. M. Peter, *J. Electroanal. Chem.* **1995**, *396*, 219–226.
- [20] J. E. Randles, *Discuss. Faraday Soc.* **1947**, *1*, 11–19.
- [21] X. M. Song, J. M. Wu, M. Z. Tang, B. Qi, M. Yan, *J. Phys. Chem. C* **2008**, *112*, 19484–19492.
- [22] A. W. Sleight, H. y. Chen, A. Ferretti, D. E. Cox, *Mater. Res. Bull.* **1979**, *14*, 1571–1581.
- [23] G. Henkelman, A. Arnaldsson, H. Jónsson, *Comput. Mater. Sci.* **2006**, *36*, 354–360.